

HOMOGENEOUS AND TOUGHENED CELLULOSE EPOXY COMPOSITES

Xinying Deng¹, Anthony J. Kinloch², Soraia Pimenta³, Gregory T. Schueneman⁴, Stephan Sprenger⁵, Ambrose C. Taylor⁶ and Wern Sze Teo⁷

¹ Department of Mechanical Engineering, Imperial College London, London SW7 2AZ, UK

¹ Singapore Institute of Manufacturing Technology, Agency for Science, Technology and Research (A*STAR), 2 Fusionopolis Way, Innovis, #08-04, Singapore 138634, Singapore
Email: x.deng14@imperial.ac.uk

² Department of Mechanical Engineering, Imperial College London, London SW7 2AZ, UK

Email: a.kinloch@imperial.ac.uk, webpage: <http://www.imperial.ac.uk/people/a.kinloch>

³ Department of Mechanical Engineering, Imperial College London, London SW7 2AZ, UK

Email: soraia.pimenta@imperial.ac.uk, webpage: <http://www.imperial.ac.uk/people/soraia.pimenta>

⁴ The Forest Products Laboratory, U.S. Forest Service, Madison, WI 53726, USA

Email: gtschueneman@fs.fed.us, webpage:
<https://www.fs.fed.us/research/people/profile.php?alias=gtschueneman>

⁵ Evonik Nutrition & Care GmbH, Charlottenburger Straße 9, 21502 Geesthacht, Germany

Email: stephan.sprenger@evonik.com

⁶ Department of Mechanical Engineering, Imperial College London, London SW7 2AZ, UK

Email: a.c.taylor@imperial.ac.uk, webpage: <http://www.imperial.ac.uk/people/a.c.taylor>

⁷ Singapore Institute of Manufacturing Technology, Agency for Science, Technology and Research (A*STAR), 2 Fusionopolis Way, Innovis, #08-04, Singapore 138634, Singapore

Email: wsteo@simtech.a-star.edu.sg, webpage:
<https://www.a-star.edu.sg/simtech/Research/Researcher-Portfolio/tid/176/Teo-Wern-Sze.aspx>

Keywords: Cellulose, Dispersion, Toughening mechanisms, Fracture energy, Resin Infusion under Flexible Tooling (RIFT).

ABSTRACT

Homogeneous and toughened cellulose-epoxy polymers were made by modifying an anhydride-cured epoxy with two green modifiers, microcrystalline cellulose (MCC) and cellulose nanocrystals (CNC). Without silane treatment, the MCC and CNC particles sedimented in the epoxy resin and formed either a gradient polymer or two distinct layers. This problem was resolved by the addition of (3-glycidyloxypropyl)trimethoxysilane (GPTMS) during the three-roll mill process, which was able to act as a coupling agent between the MCC or CNC and the epoxy, to give a modified epoxy containing homogeneously dispersed cellulose particles. The addition of MCC or CNC decreased the glass transition temperature of the epoxy, but doubled the fracture energy. By comparison, the addition of 10 wt% of nanosilica only gave a 57% increase in fracture energy. The toughening mechanisms of the MCC-epoxy and CNC-epoxy were identified to be crack deflection, pull-out and debonding of the cellulose particles, which was followed by plastic void growth. The modified Halpin-Tsai model was used to predict the increase in modulus and showed good agreement with the experimental modulus values. Analytical modelling of the fracture energies showed that particle debonding and particle pull-out contributed to the increased toughness, but the main toughening contributions were due to plastic void growth for CNC-epoxy and both plastic void growth and crack deflection for MCC-epoxy. In addition, plain-weave long glass fibre (GF) composite was manufactured with MCC using resin infusion under flexible tooling (RIFT). The interlaminar fracture energy of the composite was measured and it was found that the

increase in toughness in the epoxy polymer was not translated to the composite. This was thought to be due to the silane that was used to treat the MCC-epoxy system migrating to the glass fibre surface and improved the fibre-matrix adhesion. This reduced the amount of fibre bridging and fibre pull-out, thus reducing the mode I interlaminar fracture energy of the MCC-epoxy glass fibre composite.

1 INTRODUCTION

Nanocellulose is a promising modifier for composite materials due to its excellent properties, such as a high stiffness and crystallinity, and it has the added advantage of being derived from a sustainable source [1]. However, cellulose is incompatible with most polymer matrices, limiting the use of this promising green modifier. Various cellulose surface treatment methods have been explored, and have achieved a good dispersion for solvent-cast polymeric films such as polyurethane and epoxy [2-4]. However, although these methods are effective, the use of a solvent reduces the environmental friendliness. They are also difficult to scale-up and complete removal of the solvent is extremely difficult for composite parts. Thus, a novel and simple processing technique has been developed in this study, by adding a silane during the processing of the cellulose/epoxy mixture in a three-roll mill.

In this study, microcrystalline cellulose and cellulose nanocrystals were dried and used to modify an anhydride-cured epoxy polymer. Plates of bulk polymer were cast, and the thermal, mechanical and fracture properties of these materials were measured. These results were benchmarked against the properties of a nanosilica-modified epoxy, which has previously been shown to be an effective toughening agent [5]. Since this cellulose treatment method could be readily translated to fibre composite processing, a long glass fibre (GF) composite with MCC was manufactured using a resin infusion under flexible tooling (RIFT) process. The interlaminar fracture energy of the composite was measured and compared to the bulk fracture energy values to assess the effectiveness of the transfer of the increases in the toughness of the matrix. In addition, the toughening mechanisms of both modified polymers and composites were identified by microscopy of the fracture surfaces and of the deformation zone around the crack tip. Analytical models were used to predict the increases in toughness for the modified epoxy polymers and the predictions will be compared to the experimental results.

2 EXPERIMENTAL

2.1 Materials and manufacturing

The epoxy system used consisted of a stoichiometric ratio of standard diglycidyl ether of bisphenol A (DGEBA) epoxy resin with an epoxide equivalent weight (EEW) of 185 g/eq (Huntsman, Araldite LY556) and an accelerated methylhexahydrophthalic acid anhydride with an anhydride equivalent weight (AEW) of 170 g/eq (Evonik, Albidur HE600). The nanosilica-modified resin used was a 40 wt% masterbatch in DGEBA with an EEW of 295 g/eq (Evonik, Nanopox F400). Microcrystalline cellulose (MCC) and (3-glycidyloxypropyl)trimethoxysilane (GPTMS) were purchased from Sigma Aldrich. Freeze-dried cellulose nanocrystals (CNC) were provided by USDA Forest Service.

The cellulose modifiers were premixed with epoxy resin and GPTMS (ratio of GPTMS to modifier was 1:10) (but GPTMS was not added to the nanosilica-epoxy mixture) before being dispersed uniformly in the epoxy resin using a three-roll mill (Exakt Technologies, Exakt 80E). Three passes was used with a front roller speed of 180 rpm, gap size of 5 μm , and roller temperature of 22°C. For the modified bulk polymers, the CNC or MCC or nanosilica mixture was then mixed with HE600, degassed and cast into release-coated metal moulds. The epoxies were cured at 120 °C for 2 hours, followed by a post-cure of 160 °C for 2 hours. For the fibre composites, the MCC mixture or the unmodified resin was mixed with HE600, degassed and infused at 50 °C into the plain-weave glass fibre layup (Gurit, RE210D) via the RIFT process. The composites were cured at 100 °C for 2 hours, followed by a post-cure of 150 °C for 10 hours.

2.2 Thermal and mechanical characterisation

The glass transition temperature, T_g , values of the epoxy polymers were measured using a dynamic mechanical analyser (TA Instruments, Q800) in dual cantilever mode and in accordance with ISO 6721-1 [6]. At least three specimens of 60 mm by 10 mm by 3 mm were tested for each polymer using a ramp rate of 2 °C per minute from 30 °C to 200 °C and at 1 Hz. The T_g was determined to be the temperature corresponding to the $\tan \delta$ peak.

The tensile properties of the epoxy were determined through uniaxial tensile testing in accordance with ISO 527 [7] (Instron, 3369) using a clip-on extensometer to measure the strain in the gauge length (Instron, 2620-601). At least five specimens of size 1BA [8] were tested for each sample at a loading rate of 1 mm/min and the modulus was calculated over an interval of 0.05-0.25% strain. The fracture toughness and fracture energy (K_{IC} and G_{IC}) were obtained from single edge notched beam (SENB) tests performed in accordance with ISO 13586 (Instron, 3366). At least five specimens of 60 mm by 12 mm by 6 mm were tested for each system and the sharp pre-crack was made by tapping a liquid nitrogen chilled razor blade into a machined notch. The specimens were loaded at 1 mm/min. The yield behaviour of epoxy was analysed using plane strain compression (PSC) tests [9]. Polished specimens of size 40 mm by 40 mm by 3 mm were loaded between 12 mm wide parallel dies at a displacement rate of 0.1 mm/min. The results were corrected for machine and test rig compliance.

The tensile properties of the composites were determined by uniaxial tensile testing in accordance with ASTM3039 [10] (Instron, 5585) using a clip-on extensometer (Instron, 2620-601). At least five specimens of 150 mm by 15 mm by 4 mm, which were reinforced using adhesively-bonded glass fibre composite end tabs, were tested for each system at a loading rate of 2 mm per min. The mode I interlaminar fracture energy was obtained from double cantilever beam (DCB) tests in accordance with ISO15024 [11] (Instron, 5584). At least five specimens of 140 mm by 20 mm by 4 mm were tested for each sample and the specimens were pre-cracked and tested at a rate of 1 mm/min.

2.3 Imaging studies

A field-emission gun scanning electron microscope (FEGSEM) (Carl Zeiss, Sigma 300) was used to observe the fracture surfaces of the SENB samples (unmodified and modified epoxy polymers), and a SEM (Hitachi, S-3400N) was used to image the fracture surface of the DCB samples (unmodified and modified epoxy composites). The samples for FEGSEM and SEM were coated with a 10 nm thick layer of chromium or gold to prevent charging, and an accelerating voltage of 5 kV was used.

The plane-strain compression samples were loaded to just beyond the yield point and then unloaded. The unloaded samples were sectioned and polished to a thickness of 0.1 mm and were observed under crossed polarisers. Birefringence patterns would be observed for samples which exhibit shear yielding.

The fibre volume fractions of the composites were determined by analysing optical micrographs of polished cross-sections of the composites. These were prepared by casting the cross-sections of the composites into a cold-mount epoxy polymer, followed by grinding and polishing (Struers, LaboPol-21). Bright field micrographs of these polished specimens were taken using an optical microscope (Carl Zeiss, Axio Scope) and processed using GIMP software before being analysed using Image J software.

3 CELLULOSE EPOXY POLYMERS

The addition of cellulose was found to decrease the glass transition temperature of the epoxy, see Table 1, due to the diluent effect from both the silane and the moisture in MCC and CNC. The decreases agreed well with predictions using the $T_{g,s}$ of the individual components in the Fox equation [12]:

$$\frac{1}{T_g} = \frac{w_1}{T_{g,1}} + \frac{w_2}{T_{g,2}} \quad (1)$$

where w_1 and w_2 are the weight fractions of components 1 and 2 respectively and $T_{g,1}$ and $T_{g,2}$ are the glass transition temperatures of components 1 and 2 respectively. In this study, component 1 is the untreated epoxy and component 2 is the cellulose modifier or the silane.

However, this decrease did not compromise the fracture properties. Comparing the fracture energy values in Table 1, the addition of 10 wt% of nanosilica increased the value of G_C of the unmodified epoxy from 90 J/m² to 140 J/m², whereas 10 wt% of CNC and 10 wt% of MCC increased the fracture energy of the modified epoxy to 216 J/m² and 264 J/m² respectively. The fracture surfaces of 10 wt% CNC-epoxy and 10 wt% MCC-epoxy were rougher than those of the unmodified epoxy polymer, and from Figure 1, the cracks grew around the particles, the particles were pulled out from the matrix and there was a gap between the particles and the matrix. In addition, there were also holes on the fracture surfaces, which were left behind by debonded particles. Therefore, the toughening mechanisms were identified to be crack deflection, particle pull-out, and particle debonding, followed by plastic void growth of the epoxy.

	T_g (°C)	Young's modulus (GPa)	Tensile strength (MPa)	K_C (MPa m ^{1/2})	G_C (J/m ²)
Unmodified epoxy	157.2 ± 0.3	2.87 ± 0.05	84.4 ± 0.2	0.54 ± 0.09	89.6 ± 28.3
Epoxy with GPTMS	150.2 ± 0.3	2.96 ± 0.07	84.1 ± 2.6	0.56 ± 0.02	93.3 ± 7.8
10 wt% silica-epoxy	155.6 ± 0.3	3.04 ± 0.14	85.8 ± 1.2	0.70 ± 0.07	140.7 ± 28.8
10 wt% CNC-epoxy	136.5 ± 1.2	3.89 ± 0.13	55.2 ± 2.9	0.98 ± 0.05	215.6 ± 23.3
10 wt% MCC-epoxy	147.0 ± 0.5	3.39 ± 0.04	66.5 ± 2.6	1.01 ± 0.05	264.0 ± 26.6

Table 1: Thermal, mechanical and fracture properties for unmodified and modified bulk epoxy polymers. (Mean ± SD shown.)

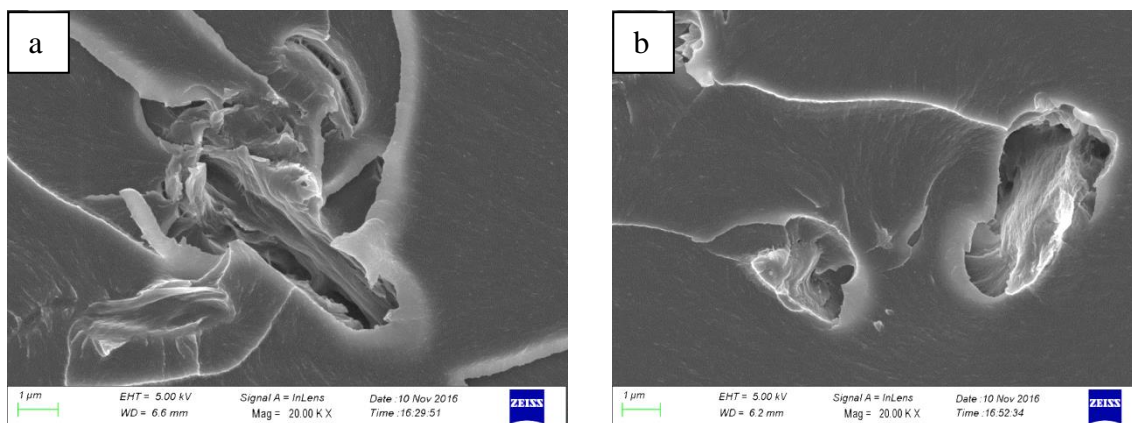


Figure 1: FEGSEM images of fracture surfaces of (a) 10 wt% MCC-epoxy and (b) 10 wt% CNC-epoxy.

The plane strain compression (PSC) results (see Figure 2) showed that strain softening was not observed for either the MCC-epoxy and CNC-epoxy polymers, which implied that the MCC and CNC particles apparently restricted the movement of the epoxy polymer chains and did not allow the matrix to deform and form shear bands [13]. Furthermore, birefringence patterns were observed for the neat epoxy and 10 wt% nanosilica-epoxy PSC samples but birefringence patterns were not observed for the MCC-epoxy and CNC-epoxy PSC samples (see Figure 3). Therefore, shear yielding did not contribute to the toughening effect observed in MCC-epoxy and CNC-epoxy polymers. This is consistent with the observations by Hsieh, whereby rod-like nanoparticles in the modified epoxy prevented the polymer from undergoing strain softening, and hence, did not allow the matrix to undergo shear yielding [14].

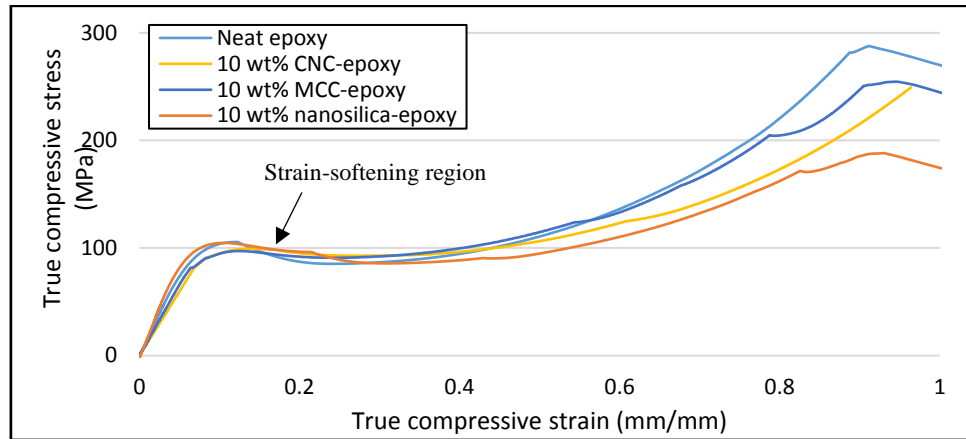


Figure 2: Plane strain compression results of bulk epoxy polymers.



Figure 3: Crossed polariser images of PSC samples loaded just beyond the yield point for (a) neat epoxy, (b) 10 wt% nanosilica-epoxy, (c) 10 wt% MCC-epoxy and (d) 10 wt% CNC-epoxy.

4 CELLULOSE EPOXY COMPOSITES

To assess the effectiveness of the transfer of the increase in the toughness of the matrix to fibre composites, a continuous glass-fibre composite with MCC was manufactured using a resin infusion under flexible tooling (RIFT) process. The tensile and interlaminar fracture energy results from the glass fibre composites are summarised in Table 2. The addition of 10 wt% MCC did not alter the Young's modulus of the composite, which was as expected since the stiffness properties of composites are fibre-dominated [15]. However, there was a slight decrease in tensile strength due to the presence of some large particles, which was consistent with the bulk polymer results (see Table 1), and the fibre volume fraction of the 10 wt% MCC-epoxy composite was lower than the unmodified epoxy composite.

	<i>Fibre volume fraction</i>	<i>Young's modulus (GPa)</i>	<i>Tensile strength (MPa)</i>	<i>Initiation G_C (J/m²)</i>	<i>Propagation G_C (J/m²)</i>
<i>Unmodified epoxy glass fibre composite</i>	0.40 ± 0.06	19.3 ± 0.9	261 ± 16	598 ± 85	738 ± 74
<i>10 wt% MCC-epoxy glass fibre composite</i>	0.36 ± 0.08	19.3 ± 1.1	226 ± 8	393 ± 72	552 ± 34

Table 2: Fibre volume fraction, mechanical and fracture properties for the unmodified and MCC-epoxy fibre composites. (Mean \pm SD shown.)

The G_C values were much larger than the bulk epoxy values (see Table 1 and Table 2), which was expected to be due to the additional fibre toughening mechanisms that were not present in the bulk epoxy [16]. The fracture surfaces of the DCB specimens had either fibres sticking out of plane or epoxy surfaces that were left behind by pulled out fibres, see Figure 4(a) and 4(b), and fibre bridging was also observed during DCB testing. Hence, the toughening mechanisms identified for the unmodified epoxy composite and the 10 wt% MCC-epoxy composite were fibre bridging and fibre pull-out. In addition, the decrease in the interlaminar fracture toughness observed in 10 wt% MCC-epoxy glass fibre composite compared to the unmodified epoxy composite, see Table 2, could be attributed to the improved interfacial adhesion between the glass fibre and the epoxy matrix as shown in Figure 4(b). The fibres in the unmodified epoxy composite had little polymer residue on them, which indicated that

the adhesion between the glass fibre and the epoxy matrix was poor (see Figure 4(a)). On the other hand, in the process of manufacturing 10 wt% MCC-epoxy glass fibre composite, GPTMS was added to improve the adhesion between MCC and epoxy, which resolved the sedimentation issue that was observed in untreated MCC-epoxy. However, it is possible that GPTMS migrated to the surface of the glass fibres, and thus increased the interfacial adhesion between the fibres and the epoxy matrix. It was clear that there were fewer fibres sticking out of the fracture surface for the 10 wt% MCC-epoxy composite compared to the unmodified epoxy composite, which indicated that the improved adhesion between the glass fibre and epoxy matrix made it more difficult for fibre bridging and fibre pull-out to occur. Therefore, the interlaminar fracture toughness of the 10 wt% MCC-epoxy composite was reduced as compared to the unmodified epoxy composite.

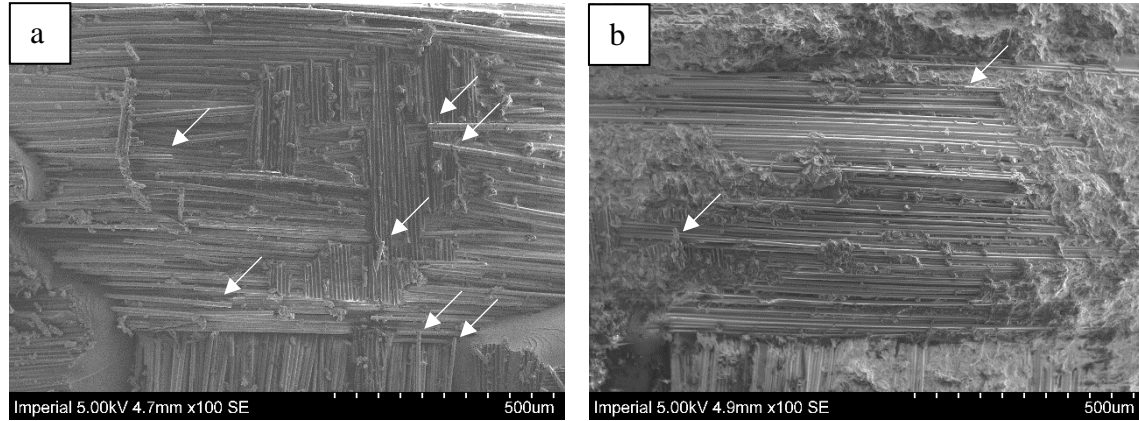


Figure 4: SEM images of fracture surface of the crack propagation region of (a) unmodified epoxy glass fibre composite and (b) 10 wt% MCC-epoxy glass fibre composite.
(Note: Fibres sticking out of plane are identified using white arrows)

5. ANALYTICAL MODELLING

5.1 Analytical modelling of the modulus

The Halpin-Tsai model is commonly used to predict modulus for particulate filled polymers and composites. A shape factor, ξ , was introduced and it was suggested to be twice the aspect ratio of the particles. The aspect ratio (A) is calculated by dividing the particle length (l_p) by twice of the particle radius (r_p) in Table 3. The modulus is given by [17]:

$$E = E_m \left(\frac{1 + \eta \xi v_f}{1 - \eta v_f} \right) \quad (2)$$

$$\eta = \frac{\frac{E_p}{E_m} - 1}{\frac{E_p}{E_m} + \xi} \quad (3)$$

where E_p is the modulus of the particles, E_m is the modulus of the matrix, and v_f is the volume fraction of the particles.

Particle	Nanosilica	MCC	CNC
<i>Particle radius (nm), r_p</i>	10	2500	12
<i>Particle length (nm), l_p</i>	20	20000	200
<i>Young's modulus (GPa)</i>	70 [18]	25 [19]	114 [20]

Table 3: Parameters used in the Halpin-Tsai prediction of the Young's modulus of the modified bulk epoxy polymers.

In the present study the particles are not aligned to the loading direction, therefore the moduli are expected to be lower than the Halpin-Tsai predictions. Using laminate theory, Van Es [21] showed that

the modulus of modified epoxy with rod-like particles with a random orientation in the Halpin-Tsai model is given by:

$$E = 0.184 E_{//} + 0.816 E_T \quad (4)$$

where the parallel, $E_{//}$, and transverse, E_T , moduli are calculated using Equation 2 with $\xi = 2$ for E_T and $\xi = 2A/3$ for $E_{//}$. This will be referred to as the modified Halpin-Tsai model.

Since the moduli of the particles were larger than the modulus of the epoxy, the moduli of the modified epoxy were expected to increase [22]. Indeed, both of the analytical models predicted that the modulus would increase when these modifiers were added to epoxy but only the modified Halpin-Tsai model agreed well with the experimental values for the MCC-epoxy and CNC-epoxy (see Figure 6). CNC and MCC are rod-like particles and were likely to be randomly orientated in the modified epoxy systems, which was confirmed by the close agreement between the predicted and experimental modulus results.

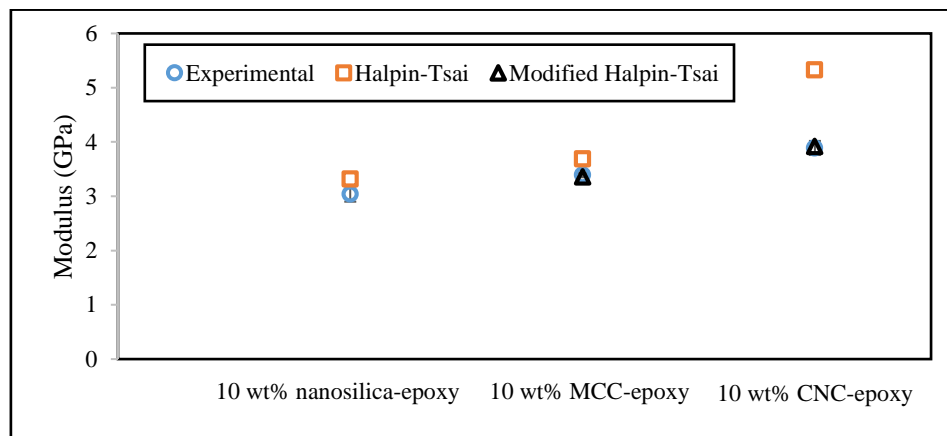


Figure 5: Experimental and predicted modulus values of modified bulk epoxy.

5.2 Analytical modelling of the fracture energy

5.2.1 The basic approach

Huang and Kinloch [23] proposed a model to predict the fracture energy of any modified epoxy from the sum of the fracture energy of the unmodified epoxy and the toughening contributions from the modifiers:

$$G_C = G_{CU} + \Psi \quad (5)$$

where G_{CU} is the fracture energy of the unmodified epoxy, and Ψ is the sum of the fracture energy contributions from the toughening mechanisms. The toughening mechanisms that will be discussed are shear band yielding, plastic void growth, crack deflection, particle debonding and pull-out.

The fracture energy contribution from shear band yielding, ΔG_s , is given by [23]:

$$\Delta G_s = 0.5 v_f \sigma_{yc} \gamma_f F'(r_y) \quad (6)$$

where v_f is the volume fraction of the modifier, σ_{yc} and γ_f are the true compressive yield stress and true failure strain of the modified epoxy measured from the plane-strain compression test, and $F'(r_y)$ is defined as [24]:

$$F'(r_y) = r_y \left[\left(\frac{4\pi}{3v_f} \right)^{\frac{1}{3}} \left(1 - \frac{r_p}{r_y} \right)^3 - \frac{8}{5} \left(1 - \frac{r_p}{r_y} \right) \left(\frac{r_p}{r_y} \right)^{\frac{5}{2}} - \frac{16}{35} \left(\frac{r_p}{r_y} \right)^{\frac{7}{2}} - 2 \left(1 - \frac{r_p}{r_y} \right)^2 + \frac{16}{35} \right] \quad (7)$$

where r_p is the radius of the particles, and r_y is the radius of the plastic zone of the modified epoxy. The value of r_y is given by:

$$r_y = K_p^2 \left(1 - \frac{\mu_m}{\sqrt{3}}\right)^2 (r_{yu}) \quad (8)$$

where μ_m is a pressure-dependent yield stress material constant which is taken to be 0.2 [25] and r_{yu} is the radius of the plane strain plastic zone of unmodified epoxy at fracture, which is given by [26]:

$$r_{yu} = \frac{1}{6\pi} \left(\frac{K_{CU}^2}{\sigma_{yt}^2}\right) \quad (9)$$

where K_{CU} is the fracture toughness of the unmodified epoxy and σ_{yt} is the tensile yield strength of the unmodified epoxy.

The von Mises stress concentration factor around a rigid particle, K_p , is defined as [18]:

$$K_p = 0.59v_f + 1.65 \quad (10)$$

The plastic void growth contribution to the fracture energy can be calculated using [23]:

$$\Delta G_v = \left(1 - \frac{\mu_m^2}{3}\right) (v_{fv} - v_f) \sigma_{yc} r_{yu} K_{vm}^2 \quad (11)$$

where σ_{yc} is the compressive yield strength of the unmodified epoxy respectively, and K_{vm} is the von Mises stress concentration factor for a void, which varies linearly with volume fractions and the value is 2.11 for the volume fraction studied [27]. Assuming that there will be void growth for all particles and all the particles will undergo the full extent of void growth,

$$r_v = (1 + \gamma_f) r_p \quad (12)$$

$$l_v = (1 + \gamma_f) l_p \quad (13)$$

where r_p is the radius of the particle, l_v is the length of a void, l_p is the radius of a void, r_v . The volume fraction of voids, v_{fv} , is given by:

$$v_{fv} - v_f = v_f \left[(1 + \gamma_f)^3 - 1 \right] \quad (14)$$

The equation for the volume fraction of the voids was found to be the same for spherical and rod-like particles. The fracture toughness and fracture energy of the unmodified epoxy was determined from the SENB tests to be 0.54 MPa m^{1/2} and 90 J/m² respectively. The tensile yield strength of the unmodified epoxy was calculated from plane strain compression tests and was found to be 81.9 MPa [23]. These values agree well with those in the literature [28]. The true failure strain of the unmodified epoxy was taken to be 0.62 [14].

5.2.2 Additional toughening contributions for rod-like particles

CNC and MCC are rod-like particles and their toughening effect could also be due to crack deflection, pull-out and debonding of the particles [14].

The energy contribution from particle debonding is [15]:

$$\Delta G_{ab} = \int_0^{l_d} \frac{N_p}{l_d} \pi 2r_p x^2 G_{if} dx \quad (15)$$

$$N_p = \frac{v_f}{\pi r_p^2} \quad (16)$$

where l_d is the debonded particle length, which is half of the particle length and G_{if} is the interfacial fracture energy and is taken to be 3.62 J/m² [29] since the interfacial fracture energy for epoxy/cellulose particles is similar to polylactic acid/cellulose particles. . Thus, Equation 15 becomes:

$$\Delta G_{db} = \frac{l_p}{2r_p} v_f G_{if} \quad (17)$$

The fracture energy contribution from the MCC/CNC pull-out mechanism is given by [15]:

$$\Delta G_{po} = \int_0^{\frac{l_p}{2}} \frac{N_p}{l_p} \pi r_p x^2 \tau_i dx \quad (18)$$

where l_p and r_p are the particle length and radius respectively, N_p is the number of particles per unit area as defined in Equation 16 and τ_i is the interfacial shear strength.

It was observed that majority of the MCC/CNC particles split into finer fibre bundles and thus, the effective pull-out length could not be determined from the FEGSEM images of the fracture surface (see Figure 1). Hence, the maximum possible pull-out length, which was half of the particle length was used to determine the energy contribution from the particle pull-out mechanism. Thus, Equation 18 becomes:

$$\Delta G_{po} = \frac{v_f \left(\frac{l_p}{2}\right)^2 \tau_i}{3r_p} \quad (19)$$

where τ_i is the interfacial shear strength. Asadi et al. [30] measured the interfacial shear strength of CNC-coated glass fibre epoxy composite and the highest CNC loading used was 5 wt%, which gave an interfacial shear strength of 16 MPa, and this value was used to calculate the pull-out fracture energy contribution for both MCC and CNC as they have similar surface chemistry.

The fracture energy contribution from the crack deflection mechanism (ΔG_{cd}) is described by the Faber and Evans model. The deflection of the crack front when it hits a particle is mixed mode, requiring more energy to move a longer distance, and the toughening effect and the full equations are described by Faber and Evans [31].

5.2.3. Predicting fracture energy for modified epoxy polymers

Different modifiers exhibit different fracture mechanisms and even when they do exhibit a certain fracture mechanism, not all of the particles will exhibit that particular fracture mechanism. Hsieh accounted for this by the product of the theoretical fracture energy contribution from the mechanisms and the volume fraction for particles observed experimentally to be exhibiting these mechanisms [14]. In the case of nanosilica-epoxy, although the crack growth originates from particle debonding, the fracture contribution from particle debonding was <1% of the fracture energy and only 5 % of the particles were found to have debonded. Therefore, the contribution from debonding was negligible and subsequent matrix shear yielding and plastic void growth was found to be the main toughening contributors for nanosilica-epoxy [5, 32, 33]. This was consistent with literature but Hsieh found that 15 % of the nanosilica particles debonded and exhibited plastic void growth [14]. Hence, the upper limit and lower limit of the fracture energy predictions for nanosilica-epoxy was set to be for the case with 15 % and 5 % of debonded nanosilica particles respectively. In the case of MCC-epoxy and CNC-epoxy, the upper limit of the fracture energy predictions was set to be when all the particles are assumed to have reached the full extent of plastic void growth and the lower limit was set to be when all the particles reached the actual average measured void growth (see Figure 6). The actual average measured void growth for MCC-epoxy and CNC-epoxy were $1.37 r_p$ and $1.43 r_p$ respectively. The compressive yield stress values used in fracture energy predictions of nanosilica-epoxy, MCC-epoxy and CNC-epoxy were 105 MPa, 93 MPa and 102 MPa respectively. In addition, crack deflection was not considered for CNC-epoxy as the particle sizes are not large enough for the crack deflection mechanism to occur [34].

Toughening mechanisms were identified in nanosilica-epoxy, CNC-epoxy and MCC-epoxy through fractography and are summarised in Equations 20-22. The predicted and experimental fracture energies of the modified epoxy polymers are shown in Figure 6.

$$G_{nanosilica-epoxy} = G_{CU} + \Psi_{nanosilica} = G_{CU} + \Delta G_s + \Delta G_v \quad (20)$$

$$G_{MCC-epoxy} = G_{CU} + \Psi_{MCC} = G_{CU} + \Delta G_{cd} + \Delta G_{po} + \Delta G_{db} + \Delta G_v \quad (21)$$

$$G_{CNC-epoxy} = G_{CU} + \Psi_{CNC} = G_{CU} + \Delta G_{po} + \Delta G_{db} + \Delta G_v \quad (22)$$

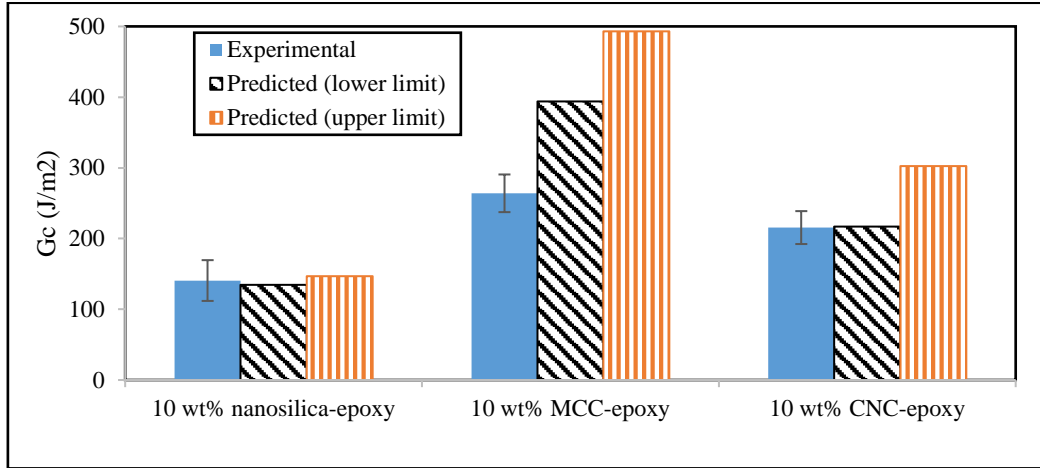


Figure 6: Fracture energy predictions and experimental results for the modified epoxy polymers.

In general, the predicted fracture energies of the modified epoxy polymers were reasonably close to the experimental values, except for 10 wt% MCC-epoxy polymer. The fracture energy prediction agreement for the 10 wt% MCC-epoxy polymer was relatively poor because the Faber and Evans model over-predicts the fracture energy contribution by the crack deflection mechanism, which is consistent with the literature [22]. In addition, the predicted fracture energy was closer to the lower limit for 10 wt% CNC-epoxy polymer, which showed that CNC particles did not undergo full extent of void growth and the actual void growth was close to the average measured void growth from FEGSEM images. Furthermore, the energy contributions from the particle debonding and pull-out mechanisms were small for the CNC-epoxy and MCC-epoxy, and thus, the main toughening contribution for CNC-epoxy was only due to plastic void growth of the matrix around the particles and the main toughening contributions for the MCC-epoxy were crack deflection and plastic void growth of the matrix around the particles.

6 CONCLUSIONS

Microcrystalline cellulose (MCC) and cellulose nanocrystals (CNC) were successfully used to modify an anhydride-cured epoxy, and the sedimentation issue of MCC and CNC in epoxy was resolved by the addition of silane during the three-roll mill process. Although the addition of cellulose decreased the T_g of the epoxy, the fracture energy of the 10 wt% modified epoxy increased by more than 100 % compared to unmodified epoxy, whereas 10 wt% of nanosilica only gave a 57 % increase in fracture energy. The main toughening mechanisms identified by fractography were crack deflection, particle debonding and pull-out, followed by plastic void growth of the epoxy. In addition, glass fibre composites were fabricated via a RIFT process and fibre bridging and fibre pull-out were identified to be the main toughening mechanisms. The interlaminar fracture toughness of 10 wt% MCC-epoxy glass fibre composite was lower than the unmodified epoxy glass fibre composite, which was attributed to silane migration to the glass fibre surface, which improved the interface between the glass fibre and epoxy, impeding fibre bridging and fibre pull-out. The modified Halpin-Tsai model showed good agreement with the experimental moduli results and the analytical models showed reasonably good agreement with the experimental fracture energy of the modified polymers, except for 10wt% MCC-epoxy. This was due to over-prediction of the crack deflection contribution by the Faber and Evans model. Furthermore, the models showed that particle debonding and particle pull-out contributed to the toughening increment but the main toughening contribution was due to plastic void growth for the CNC-epoxy, and the main toughening contributions were due to both crack deflection and plastic void growth for the MCC-epoxy.

ACKNOWLEDGEMENTS

The authors would like to thank Agency of Science, Technology and Research, Singapore, for the scholarship for Ms. Xinying Deng.

REFERENCES

- [1] R.J. Moon, A. Martini, J. Nairn, J. Simonsen, and J. Youngblood, Cellulose nanomaterials review: Structure, properties and nanocomposites. *Chemical Society Reviews*. **40**, 2011, pp. 3941-3994, (doi: 10.1039/C0CS00108B).
- [2] Y. Habibi, Key advances in the chemical modification of nanocelluloses. *Chemical Society Reviews*. **43**, 2014, pp. 1519-1542, (doi: 10.1039/C3CS60204D).
- [3] J. Lu, P. Askeland, and L.T. Drzal, Surface modification of microfibrillated cellulose for epoxy composite applications. *Polymer*. **49**, 2008, pp. 1285-1296, (doi: 10.1016/j.polymer.2008.01.028).
- [4] N.M. Girouard, S. Xu, G.T. Schueneman, M.L. Shofner, and J.C. Meredith, Site-selective modification of cellulose nanocrystals with isophorone diisocyanate and formation of polyurethane-cnc composites. *ACS Applied Materials & Interfaces*. **8**, 2016, pp. 1458-1467, (doi: 10.1021/acsami.5b10723).
- [5] B.T. Marouf, Y.-W. Mai, R. Bagheri, and R.A. Pearson, Toughening of epoxy nanocomposites: Nano and hybrid effects. *Polymer Reviews*. **56**, 2016, pp. 70-112, (doi: 10.1080/15583724.2015.1086368).
- [6] ISO 6721-1. *Plastics — determination of dynamic mechanical properties. Part 1: General principles*. Geneva, Switzerland: ISO; 2011.
- [7] ISO 527-1. *Plastics — determination of tensile properties. Part 1: General principles*. Geneva, Switzerland: ISO; 2012.
- [8] ISO527-2. *Plastics — determination of tensile properties. Part 2: Test conditions for moulding and extrusion plastics*. Geneva, Switzerland: ISO; 2012.
- [9] J.G. Williams and H. Ford, Stress-strain relationships for some unreinforced plastics. *Journal of Mechanical Engineering Science*. **6**, 1964, pp. 405-417, (doi: 10.1243/JMES_JOUR_1964_006_055_02).
- [10] ASTM 3039. *Tensile properties of polymer matrix composite materials*. West Conshohocken, PA: ASTM International; 2014.
- [11] ISO 15024. *Fibre-reinforced plastic composites — determination of mode I interlaminar fracture toughness, G_{IC} , for unidirectionally reinforced materials*. Geneva, Switzerland.: ISO; 2001.
- [12] T.G. Fox, Influence of diluent and copolymer composition on the glass temperature of a polymer system. *Bulletin of the American Physical Society*. **1**, 1956, pp. 123.
- [13] V.V. Kozey and S. Kumar, Compression behavior of materials: Part i. Glassy polymers. *Journal of Materials Research*. **9**, 2011, pp. 2717-2726, (doi: 10.1557/JMR.1994.2717).
- [14] T.-H. Hsieh, *Properties and toughening of silica nanoparticle- and carbon nanotube-modified epoxy polymers*, PhD Thesis, Department of Mechanical Engineering, Imperial College London, 2011.
- [15] D. Hull and T. Clyne, *An introduction to composite materials*. 1996: Cambridge University Press, New York.
- [16] L. Ye and K. Friedrich, Mode I interlaminar fracture of co-mingled yarn based glass/polypropylene composites. *Composites Science and Technology*. **46**, 1993, pp. 187-198, (doi: 10.1016/0266-3538(93)90174-F).
- [17] J.C. Halpin and J.L. Kardos, The Halpin-Tsai equations: A review. *Polymer Engineering & Science*. **16**, 1976, pp. 344-352, (doi: 10.1002/pen.760160512).
- [18] F.J. Guild and R.J. Young, A predictive model for particulate-filled composite materials. *Journal of Materials Science*. **24**, 1989, pp. 298-306, (doi: 10.1007/bf00660971).
- [19] S.J. Eichhorn and R.J. Young, The Young's modulus of a microcrystalline cellulose. *Cellulose*. **8**, 2001, pp. 197-207, (doi: 10.1023/a:1013181804540).

- [20] Y.-C. Hsieh, H. Yano, M. Nogi, and S.J. Eichhorn, An estimation of the Young's modulus of bacterial cellulose filaments. *Cellulose*. **15**, 2008, pp. 507-513, (doi: 10.1007/s10570-008-9206-8).
- [21] M. Van Es, *Polymer-clay nanocomposites*, PhD Thesis, *Applied Sciences*, Delft University of Technology, 2001.
- [22] A.J. Kinloch and A.C. Taylor, The mechanical properties and fracture behaviour of epoxy-inorganic micro- and nano-composites. *Journal of Materials Science*. **41**, 2006, pp. 3271-3297, (doi: 10.1007/s10853-005-5472-0).
- [23] Y. Huang and A.J. Kinloch, Modelling of the toughening mechanisms in rubber-modified epoxy polymers. *Journal of Materials Science*. **27**, 1992, pp. 2763-2769, (doi: 10.1007/bf00540703).
- [24] T.H. Hsieh, A.J. Kinloch, K. Masania, J. Sohn Lee, A.C. Taylor, and S. Sprenger, The toughness of epoxy polymers and fibre composites modified with rubber microparticles and silica nanoparticles. *Journal of Materials Science*. **45**, 2010, pp. 1193-1210, (doi: 10.1007/s10853-009-4064-9).
- [25] J.N. Sultan and F.J. McGarry, Effect of rubber particle size on deformation mechanisms in glassy epoxy. *Polymer Engineering & Science*. **13**, 1973, pp. 29-34, (doi: 10.1002/pen.760130105).
- [26] C.B. Bucknall and I.K. Partridge, Phase separation in epoxy resins containing polyethersulphone. *Polymer*. **24**, 1983, pp. 639-644.
- [27] F.J. Guild and R.J. Young, A predictive model for particulate filled composite materials. *Journal of Materials Science*. **24**, 1989, pp. 2454-2460, (doi: 10.1007/bf01174511).
- [28] H.M. Chong, *Toughening mechanisms of block copolymer and graphene nanoplatelet modified epoxy polymers*, PhD Thesis, *Department of Mechanical Engineering*, Imperial College London, 2015.
- [29] I. Siró, Y. Kusano, K. Norrman, S. Goutianos, and D. Plackett, Surface modification of nanofibrillated cellulose films by atmospheric pressure dielectric barrier discharge. *Journal of Adhesion Science and Technology*. **27**, 2013, pp. 294-308, (doi: 10.1080/01694243.2012.705522).
- [30] A. Asadi, M. Miller, R. Moon, and K. Kalaitzidou, Improving the interfacial and mechanical properties of short glass fiber/epoxy composites by coating the glass fibers with cellulose nanocrystals. *Express Polym Lett*. **10**, 2016, pp. 587-97, (doi: 10.3144/expresspolymlett.2016.54).
- [31] K.T. Faber and A.G. Evans, Crack deflection processes—i. Theory. *Acta Metallurgica*. **31**, 1983, pp. 565-576, (doi: 10.1016/0001-6160(83)90046-9).
- [32] D. Carolan, A. Ivankovic, A.J. Kinloch, S. Sprenger, and A.C. Taylor, Toughening of epoxy-based hybrid nanocomposites. *Polymer*. **97**, 2016, pp. 179-190, (doi: 10.1016/j.polymer.2016.05.007).
- [33] A.J. Kinloch, *Adhesion and adhesives: Science and technology*. 2012: Springer Science & Business Media, London.
- [34] D.J. Green, P.S. Nicholson, and J.D. Embury, Fracture of a brittle particulate composite. *Journal of Materials Science*. **14**, 1979, pp. 1657-1661, (doi: 10.1007/bf00569287).